Proceedings of the 6th International Conference on Gas Hydrates (ICGH 2008),
Vancouver, British Columbia, CANADA, July 6-10, 2008.

EFFECT OF OVERPRESSURE ON GAS HYDRATE DISTRIBUTION

Gaurav Bhatnagar, Walter G. Chapman, George J. Hirasaki*
Department of Chemical & Biomolecular Engineering
Rice University
6100 Main St., Houston, TX, 77005
USA

Gerald R. Dickens, Brandon Dugan
Department of Earth Science
Rice University
6100 Main St., Houston, TX, 77005
USA

ABSTRACT

The effect of overpressure on gas hydrate and free gas distribution in marine sediments is studied using a one-dimensional numerical model that couples sedimentation, fluid flow, and gas hydrate formation. Natural gas hydrate systems are often characterized by high sedimentation rates and/or low permeability sediments, which can lead to pore pressure higher than hydrostatic (overpressure). To quantify the relative importance of these two factors, we define a dimensionless sedimentation-compaction group, N_{sc}, that compares the absolute permeability of the sediments to the sedimentation rate. Higher values of N_{sc} mean higher permeability or low sedimentation rate which generally yield hydrostatic pore pressure. Conversely, lower values of N_{sc} generally create pore pressure greater than hydrostatic. Simulation results show that decreasing N_{sc} not only increases pore pressure above hydrostatic values, but also lowers the lithostatic stress gradient and gas hydrate saturation. This occurs because overpressure results in lower effective stress, causing higher porosity and lower bulk density of the sediment. This leads to higher sediment velocity through the gas hydrate stability zone, thereby reducing the mass accumulation of methane and gas hydrate in the pore space. Effect of overpressure on depth of the gas hydrate stability zone is also studied.

Keywords: gas hydrate, overpressure, sedimentation-compaction, numerical modeling

NOMENCLATURE

c_i^j	Mass fraction of component i in phase j
$c_{m,eqb}^l$	Methane solubility at base of GHSZ
D_m	Methane diffusivity in seawater
Da	Damkohler number
g	Acceleration due to gravity
N_{sc}	Sedimentation-compaction group
k	Absolute sediment permeability
k_0	Absolute sediment permeability at seafloor
k_{rj}	Relative permeability of phase j
L_t	Depth to the base of the GHSZ
L_ϕ	Characteristic depth of compaction

* Corresponding author: Phone: +1 713 348 5416 Fax +1 713 348 5478 E-mail: gjh@rice.edu

M_i Molecular weight of component i
Pe_1 Peclet number
p_j Pressure of phase j
S_j Saturation of phase j
$\dot{S}$ Sedimentation rate at the seafloor
t Time
$U_{f,sed}$ Fluid flux due to sedimentation
v_j Velocity of phase j
z Depth below seafloor
α Organic carbon content
α_0 Organic carbon content at seafloor
β Normalized organic content at seafloor
γ, η Reduced porosity parameters
λ Methanogenesis reaction rate
μ_j Viscosity of phase j
ρ_j Density of phase j
σ_v Vertical effective stress
σ_ϕ Characteristic stress for compaction
ϕ Porosity
ϕ_0 Porosity at seafloor
ϕ_∞ Porosity at great depths

Subscripts/superscripts:
g Gas phase
h Hydrate phase
l, w Water phase or component
m Methane component
s Sediment phase

INTRODUCTION

Gas hydrate systems are sometimes characterized by overpressure, i.e. pore water pressure higher than hydrostatic. This is particularly evident at settings dominated by low permeability silts/clays, e.g., Blake Ridge [1,2]. Over geologic timescales, continuous sedimentation causes increase in the overburden, resulting in consolidation of sediments [3,4,5]. Overpressure can develop in such systems if pore water cannot be expelled from the pore space fast enough and, instead, supports some of the overburden. Since permeability controls this rate of pore water expulsion, sediments with low permeability can develop overpressure [4,5]. Alternatively, overpressure can also develop in sediments with relatively high permeability if the sedimentation rate is fast, i.e. increase in overburden is faster than rate of pore water expulsion [3].

Overpressure impacts the behavior of gas hydrate systems in several ways. For example, the maximum thickness of the free gas layer below the base of the gas hydrate stability zone (GHSZ) depends on the magnitude of overpressure [2,6,7]. The length of a free gas column sealed by overlying gas hydrate is regulated by the difference between pore water pressure and lithostatic stress. Thus, higher pore water pressures imply that relatively short connected gas columns can develop before fracturing or shear failure occurs, thereby causing a sudden release of free gas [2,6,7]. Conversely, relatively long connected gas columns can form when water overpressure is zero.

Overpressure also affects sediment and gas hydrate velocity through the GHSZ. At hydrostatic pore pressures, sediments lose porosity due to relatively high effective stresses driving consolidation. Overpressure reduces the effective stress acting on the sediments, which precludes consolidation and preserves high porosity. This leads to faster sediment velocity through the GHSZ. In a gas hydrate system dominated by in-situ biogenic methane supply, this increase in sediment velocity curtails the amount of organic carbon converted to methane within the GHSZ. This occurs because the organic carbon is also progressively buried deeper with the sediment. Additionally, increased sediment velocity also reduces the residence time of gas hydrate in the GHSZ. These two mechanisms can cause overpressure to result in relatively lower gas hydrate and free gas saturations at steady-state.

Overpressure can also change the gas hydrate stability regime and extend the base of the GHSZ to greater depths below the seafloor. However, we show through numerical simulations that this increase in depth of the GHSZ due to overpressure is relatively small, even when pore pressures approach the lithostatic stress.

We have previously developed generalized dimensionless numerical models to study gas hydrate and free gas distribution in marine

sediments [8,9]. However, these models assumed hydrostatic conditions. In this paper, we explicitly incorporate water pressure through the use of Darcy's law in a consolidating medium. This allows us to model overpressure development and study its effect on gas hydrate/free gas saturation.

NON-HYDROSTATIC CONSOLIDATION IN GAS HYDRATE SYSTEMS

We develop a one-dimensional numerical model to simulate overpressure generation in marine gas hydrate systems and study the parameters governing this process. Darcy's law is used to model fluid flow relative to the consolidating sediment. We only focus on the effects of overpressure due to sedimentation-consolidation and sediment permeability in this paper. Consequently, we assume a relatively higher value of critical gas saturation of 10%, which ensures that free gas will remain immobile.

Mass balances

The water, methane, sediment and organic mass balances are written as:

Water Balance:

$$\frac{\partial}{\partial t}\left[\phi S_w c_w^l \rho_w + \phi S_h c_w^h \rho_h\right] + \frac{\partial}{\partial z}\left[\phi S_w c_w^l \rho_w v_w + \phi S_h c_w^h \rho_h v_s\right] = 0 \quad (1)$$

Methane Balance:

$$\frac{\partial}{\partial t}\left[\phi S_w c_m^l \rho_w + \phi S_h c_m^h \rho_h + \phi S_g c_m^g \rho_g\right] + \frac{\partial}{\partial z}\left[\phi S_w c_m^l \rho_w v_w + \phi S_h c_m^h \rho_h v_s + \phi S_g c_m^g \rho_g v_s\right] = \frac{\partial}{\partial z}\left[\phi S_w D_m \rho_w \frac{\partial c_m^l}{\partial z}\right] + \frac{M_{CH_4}}{M_{org}} \rho_s \lambda (1-\phi)\alpha \quad (2)$$

Sediment Balance:

$$\frac{\partial}{\partial t}\left[(1-\phi)\rho_s\right] + \frac{\partial}{\partial z}\left[(1-\phi)\rho_s v_s\right] = 0 \quad (3)$$

Organic Balance:

$$\frac{\partial}{\partial t}\left[(1-\phi)\rho_s\right]\alpha + \frac{\partial}{\partial z}\left[(1-\phi)\rho_s v_s \alpha\right] = -\rho_s \lambda (1-\phi)\alpha \quad (4)$$

Constitutive relationships

We now list the constitutive relationships used in this formulation.

Darcy's law for water flux in a consolidating medium [10]:

$$S_w \phi (v_w - v_s) = -\frac{k k_{rw}}{\mu_w}\left(\frac{\partial p_w}{\partial z} - \rho_w g\right) \quad (5)$$

We assume absolute permeability of sediment is a power law function of porosity [11]:

$$k = k_0 \left(\frac{\phi}{\phi_0}\right)^8 \quad (6)$$

Water relative permeability in the presence of gas hydrate is modeled assuming pore-filling structure for the hydrate [12]:

$$k_{rw} = 1 - S_h^2 + \frac{2(1-S_h)^2}{\ln(S_h)} \quad (7)$$

Water relative permeability in the presence of free gas is [10]:

$$k_{rw} = k_{rw}^0 \left(S_w^*\right)^4, \text{ where } S_w^* = \frac{S_w - S_{wr}}{1 - S_{wr}} \quad (8)$$

We assume porosity is controlled by the effective stress [13]:

$$\phi = \phi_\infty + (\phi_0 - \phi_\infty) e^{-\frac{\sigma_v - p_w}{\sigma_\phi}} \quad (9)$$

Lithostatic stress gradient can be written as a function of densities and porosity as:

$$\frac{\partial \sigma_v}{\partial z} = \left[(1-\phi)\rho_s + \phi \rho_w\right] g \quad (10)$$

Normalized variables and dimensionless groups

The above equations are now written in dimensionless form. Reduced porosities are:

$$\tilde{\phi} = \frac{\phi - \phi_\infty}{1 - \phi_\infty},\ \eta = \frac{\phi_0 - \phi_\infty}{1 - \phi_\infty},\ \gamma = \frac{1 - \phi_\infty}{\phi_\infty} \tag{11}$$

The Peclet and Damkohler numbers are defined as:

$$Pe_1 = \frac{U_{f,sed} L_t}{D_m},\ Da = \frac{\lambda L_t^2}{D_m} \tag{12}$$

We also define a dimensionless group relating the absolute sediment permeability and the sedimentation rate at the seafloor:

$$N_{sc} = \frac{k_0 \rho_w g}{\mu_w \dot{S}} \tag{13}$$

Large values of N_{sc} correspond to high sediment permeability and/or low sedimentation rate, implying hydrostatic pressures. Conversely, low values of N_{sc} imply low permeability and/or high sedimentation rate, thereby causing overpressure. Similar dimensionless groups have been used to model overpressure development in sedimentary basins [14,15].

The ratio of the characteristic consolidation depth to the base of GHSZ is defined by the dimensionless group, $N_{t\phi}$:

$$N_{t\phi} = \frac{L_\phi}{L_t} = \frac{\sigma_\phi / (\rho_w g)}{L_t} \tag{14}$$

The normalized methane concentrations are defined as:

$$\tilde{c}_m^l = \frac{c_m^l}{c_{m,eqb}^l},\ \tilde{c}_m^h = \frac{c_m^h}{c_{m,eqb}^l},\ \tilde{c}_m^g = \frac{c_m^g}{c_{m,eqb}^l} \tag{15}$$

Lithostatic stress (σ_v), water pressure and gas pressure are normalized by hydrostatic water pressure at the base of the GHSZ:

$$\tilde{\sigma}_v = \frac{\sigma_v}{\rho_w g L_t},\ \tilde{p}_w = \frac{p_w}{\rho_w g L_t},\ \tilde{p}_g = \frac{p_g}{\rho_w g L_t} \tag{16}$$

Dimensionless depth and time are defined as:

$$\tilde{z} = \frac{z}{L_t},\ \tilde{t} = \frac{t}{L_t^2 / D_m} \tag{17}$$

All phase densities are normalized by water density ($\tilde{\rho}_i = \rho_i / \rho_w$). Sediment velocity is normalized by the sedimentation rate at the seafloor:

$$\tilde{v}_s = \frac{v_s}{\dot{S}} \tag{18}$$

Finally, organic carbon content and initial carbon content at the seafloor are normalized as:

$$\tilde{\alpha} = \frac{\alpha}{\alpha_0},\ \beta = \frac{\alpha_0}{c_{m,eqb}^l} \tag{19}$$

The resulting dimensionless mass balances and constitutive relationships are given in the appendix.

NUMERICAL SOLUTION

The coupled dimensionless equations are solved numerically using a fully implicit finite difference formulation, with the primary variables being $\tilde{p}_w$, $\tilde{v}_s$, $\tilde{\alpha}$ and $\tilde{c}_m^l$, S_h, or S_g. Choice between $\tilde{c}_m^l$, S_h, or S_g is made according to the local thermodynamic conditions at any gridblock at any given time-step. All four mass balances are cast in residual form and the Newton-Raphson method is used to iterate on them to converge to the solution.

RESULTS

To study the effect of overpressure on gas hydrate and free gas saturation, we simulate cases with different values of the sedimentation-consolidation parameter, N_{sc}. Apart from the parameter N_{sc}, other primary simulation parameters include the Peclet number, the Damkohler number, the normalized organic carbon input and the reduced porosity parameters. Values used in the

simulations are: Pe_1 = 0.1, Da = 10, β = 3, $N_{t\phi}$ = 1, η = 6/9, and γ = 9. Seafloor parameters are chosen to be similar to the Blake Ridge region [16], with seafloor temperature of 3°C, seafloor depth of 2700 m, and geotherm of 0.04°C/m. We keep these parameters constant and only vary N_{sc} from high to low values (Figure 1). Hydrostatic pressure and lithostatic stress profiles are also provided as minimum and maximum bounds to the pore pressure, respectively.

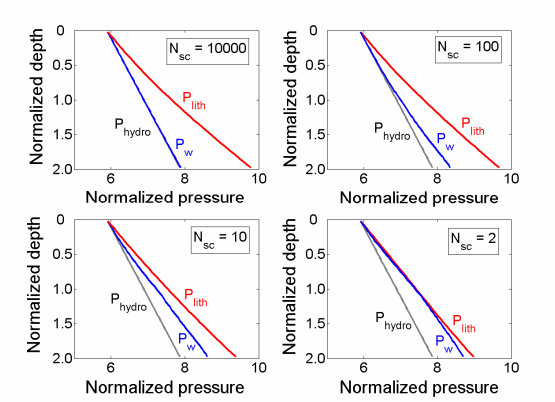

Figure 1: Effect of the sedimentation-consolidation parameter, N_{sc}, on steady-state pore pressure profiles. Each pore pressure curve is bounded by the hydrostatic pressure profile as the lower limit and the lithostatic stress profile as the upper limit.

Simulations show that relatively higher values of N_{sc} (~10^4) lead to almost hydrostatic pore pressures, whereas relatively lower N_{sc} (~1) lead to pore pressures that are close to the lithostatic limit (Figure 1). This occurs because relatively low N_{sc} values imply lower sediment permeability and/or high sedimentation rate. Either of these conditions can impede expulsion of pore water in response to increasing overburden, leading to pore pressures higher than hydrostatic values. Conversely, relatively higher values of N_{sc} imply high sediment permeability and/or low sedimentation rate. This facilitates fluid drainage, consolidation, and pore pressures that remain close to hydrostatic.

Figure 1 also reveals that the lithostatic stress at a constant depth reduces as pore pressures increases. To illustrate this more clearly, we plot pore pressure and lithostatic stress profiles corresponding to the four cases together in Figure 2. This comparison of pore pressure and lithostatic profiles show how the curves remain separated from each other at large N_{sc}. However, with lower N_{sc}, pore pressure and lithostatic curves approach each other; the pressure increases and the lithostatic stress decreases. Decreased lithostatic stress occurs because increased porosities caused by lower effective stresses acting on the sediments cause lower bulk densities of the sediment (Equation 10).

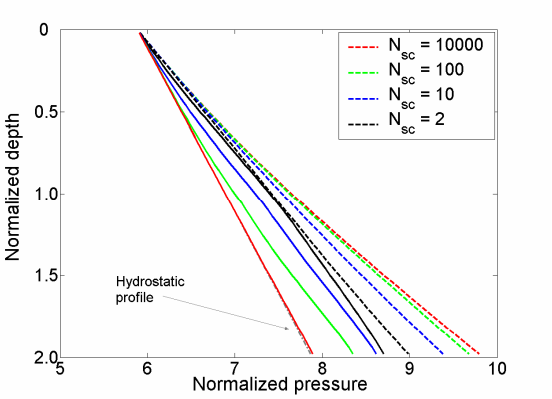

Figure 2: Pressure profiles shown in Figure 1 plotted together for all four cases. Lithostatic stress profiles (dashed curves) and the corresponding pore pressure profiles (solid curves) for the same value of N_{sc} are color-coded together.

As mentioned before, increase in pore pressure influences the thermodynamic stability of gas hydrates. Specifically, increase in pore pressure extends the depth to the base of the GHSZ deeper into the sedimentary column. This change is shown through the methane solubility curves for the same set of N_{sc} values we have simulated in (Figure 3).

We start with the case N_{sc} = 10000, which corresponds to near-hydrostatic pore pressures. According to the scaling scheme defined previously, the solubility curve for this case has a peak methane solubility equal to unity at unit normalized depth. As pore pressure increases, i.e.

N_{sc} decreases, we observe that the peak values of the solubility curves shift to higher values, with the peak itself occurring slightly deeper (Figure 3). This demonstrates that the base of GHSZ is a dynamic boundary that moves in response to the pore pressure.

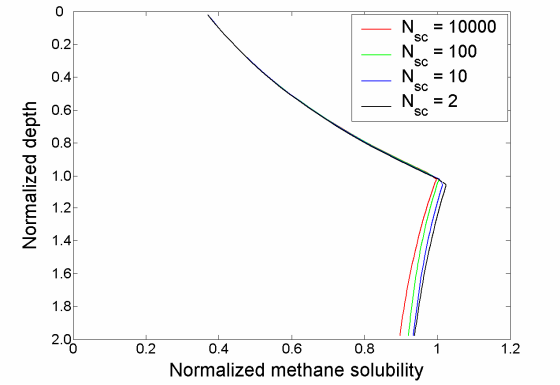

Figure 3: Effect of overpressure on methane solubility curves. Decreasing N_{sc} from 10000 to 2 causes increasing overpressure within the sediment and results in a deeper base of the GHSZ. The magnitude of this downward shift is, however, negligible even when the pore pressure is close to lithostatic.

Even when pore pressures are close to lithostatic, the downward shift in the base of the GHSZ is very small in the normalized form. When the normalized vertical depth scale (Figure 3) is converted back to the physical scale by multiplying with L_t, the depth to the base of GHSZ, this increase in the thickness of the GHSZ becomes larger, but is still relatively small. For example, for the case corresponding to almost lithostatic pore pressure, the downward shift in the base of the GHSZ is about 20 m, which, for Blake Ridge type seafloor conditions, is only about 0.7% of the water depth.

The effect of N_{sc} on steady-state gas hydrate and free gas saturation profiles is also investigated. Maximum gas hydrate and free gas saturation occur at the highest values of N_{sc}, which corresponds to hydrostatic pore pressure (Figure 4). Progressively decreasing N_{sc} leads to lower gas hydrate and free gas saturations (Figure 4). As mentioned before, relatively lower values of N_{sc} lead to higher overpressures, higher sediment porosities and faster sediment velocities, which result in lower organic carbon decay within the GHSZ and shorter residence times of hydrate and free gas in the GHSZ.

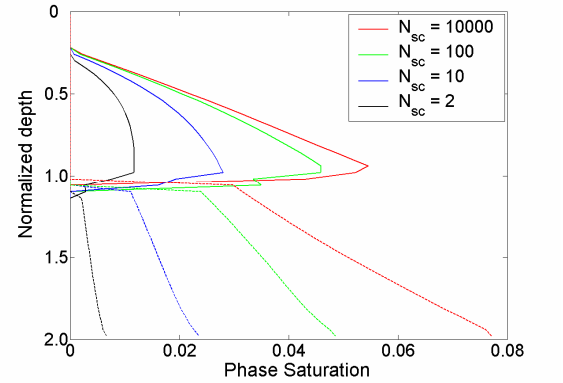

Figure 4: Effect of overpressure, characterized through N_{sc}, on steady-state gas hydrate saturation (solid curves) and free gas saturation profiles (dashed curves). Relatively smaller values of N_{sc} lead to overpressure development, higher porosities, higher sediment velocities, and lower net hydrate and free gas saturations.

However, it should be noted that hydrate and free gas saturation profiles do not give a complete picture of their amounts, because each value of N_{sc} results in a different porosity profile. Thus, although hydrate and free gas saturation within the pore space decrease on lowering N_{sc}, the corresponding increase in porosity might lead to net higher accumulation of hydrate or free gas within the sediment volume. To test this scenario, we plot the product of porosity and hydrate/free gas saturation (ϕS_j) to get the volume fraction of hydrate and free gas within the sediment (Figure 5). These profiles show that the net amount of gas hydrate or free gas saturation within the sediment also decreases on lowering N_{sc}. However, multiplying by porosity does reduce the magnitude of change observed between different cases. For example, peak hydrate saturation at the base of GHSZ decreases from about 6% to 1%, a factor of 6 change, on lowering N_{sc} from 10000 to 2. In

contrast, peak change in sediment volume fraction of hydrate goes from about 2.2% to 0.7%, a factor of 3 change, for the same decrease in N_{sc}.

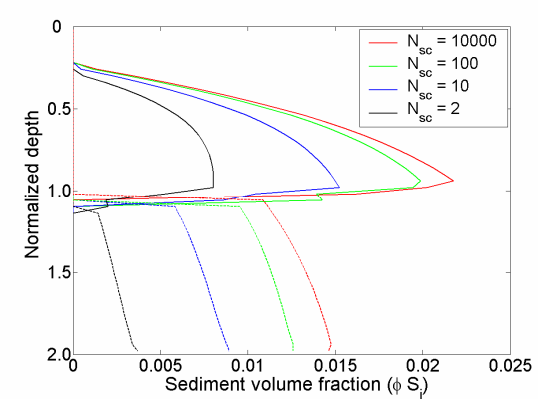

Figure 5: Effect of overpressure, characterized through N_{sc}, on steady-state gas hydrate (solid curves) and free gas (dashed curves) sediment volume fraction.

This validates our hypothesis that overpressure does lower the net amount of methane that accumulates in either hydrate or free gas phase. In other words, the decrease in hydrate and free gas saturation with increasing overpressure is not only a result of increased porosities. The effect of increased sediment and fluid velocities and lower organic carbon decay within the GHSZ has a much more significant impact on net gas hydrate and free gas accumulation.

Effect on free gas column thickness

Based on pressure profiles shown in Figures 1 and 2, it can be argued that deep connected free gas columns may result for settings characterized by high N_{sc}. In contrast, only short gas columns can form when N_{sc} is low before sediment fracture/failure occurs and vents the free gas into the ocean. Thus, from an exploration standpoint, geologic sites characterized by high permeability and low sedimentation rates (i.e., high N_{sc}) might be most suitable for targeting the free gas sealed by a hydrate layer.

CONCLUSIONS

A dimensionless numerical model for non-hydrostatic pressure compaction is developed to study the effect of overpressure on gas hydrate and free gas saturations. Non-dimensionalization of the equations lead to a sedimentation-consolidation group, N_{sc}, defined as the ratio of sediment permeability to sedimentation rate. Simulations show that relatively high values of N_{sc} (about 10^4) lead to systems close to hydrostatic pore pressure, while relatively low values of N_{sc} (~1) lead to significant overpressure in the system. Overpressure development impacts this gas hydrate system by lowering effective stresses on the sediment, causing higher porosities. Higher sediment velocities achieved due to overpressure and high porosities ultimately lead to lesser organic carbon decay, resulting in lower hydrate and free gas saturations for our set of boundary conditions, i.e., fixed seafloor depth and constant geotherm.

ACKNOWLEDGEMENTS

We acknowledge financial support form the Shell Center for Sustainability, the Kobayashi Graduate Fellowship, and the Department of Energy (DE-FC26-06NT42960).

REFERENCES

[1] Winters WJ. *Stress history and geotechnical properties of sediment from the Cape Fear Diapir, Blake Ridge Diapir, and Blake Ridge*. In: Paull CK, Matsumoto R, Wallace PJ, Dillon WP, editors. Proceedings of the Ocean Drilling Program, Scientific Results, volume 164: College Station, Texas Ocean Drilling Program, 2000. p. 421-429.

[2] Flemings PB, Liu X, Winters WJ. *Critical pressure and multiphase flow in Blake Ridge gas hydrates*. Geology 2003; 31:1057-1060.

[3] Gibson RE. *The progress of consolidation in a clay layer increasing in thickness with time*. Geotechnique 1958; 8:171-182.

[4] Wangen M. *Pressure and temperature evolution in sedimentary basins*. Geophysical Journal International 1992; 110:601-613.

[5] Dugan B, Flemings PB. *Overpressure and fluid flow in the New Jersey continental slope: implications for slope failure and cold seeps*. Science 2000; 289:288-291.

[6] Hornbach MJ, Saffer, DM, Holbrook, WS. *Critically pressured free-gas reservoirs below gas-hydrate provinces*. Nature 2004; 427:142-144.
[7] Liu XL, Flemings PB. *Dynamic multiphase flow model of hydrate formation in marine sediments*. Journal of Geophysical Research 2007; 112:B03101, doi:10.1029/2005JB004227.
[8] Bhatnagar G, Chapman WG, Dickens GR, Dugan B, Hirasaki GJ. *Generalization of gas hydrate distribution and saturation in marine sediments by scaling of thermodynamic and transport processes*. American Journal of Science 2007; 307:861-900.
[9] Bhatnagar G, Chapman WG, Dickens GR, Dugan B, Hirasaki GJ. *Sulfate-methane transition as a proxy for average methane hydrate saturation in marine sediments*. Geophysical Research Letters 2008; 35:L03611, doi:10.1029/2007GL032500.
[10] Bear J. *Dynamic of fluids in porous media*. New York: Dover Publications Inc., 1988.
[11] Smith JE. *The dynamics of shale compaction and evolution of pore-fluid pressures.* Mathematical Geology 1971; 3:239-263.
[12] Kleinberg RL, Flaum C, Griffin DD, Brewer PG, Malby GE, Peltzer ET, Yesinowski JP. *Deep sea NMR: Methane hydrate growth habitat in porous media and its relationship to hydraulic permeability, deposit accumulation, and submarine slope stability*. Journal of Geophysical Research 2003; 108(B10):2508, doi:10.1029/2003JB002389.
[13] Rubey WW, Hubbert MK. *Role of fluid pressure in mechanics of over-thrust faulting; ii. Overthrust belt in geosynclinal area of western Wyoming in light of fluid pressure hypothesis.* Geological Society of America Bulletin 1959; 70:167-206.
[14] Yang XS, Fowler AC. *Fast and slow compaction in sedimentary basins*. SIAM Journal on Applied Mathematics 1998; 59(1):365-385.
[15] Gutierrez M, Wangen M. *Modeling of compaction and overpressuring in sedimentary basins*. Marine and Petroleum Geology 2005; 22(3):351-363.
[16] Paull CK, Matsumoto R, Wallace PJ, Dillon WP, editors. Proceedings of the Ocean Drilling Program, Scientific Results, volume 164: College Station, Texas Ocean Drilling Program, 2000. p. 421-429.

APPENDIX

Dimensionless mass balances

The scaling schemes defined in the main text lead to the following form of the four mass balances, initial conditions (I.C.) and boundary conditions (B.C.).

Water Balance:

$$\frac{\partial}{\partial \tilde{t}}\left[\frac{1+\gamma\tilde{\phi}}{\gamma}\left(S_w c_w^l + S_h c_w^h \tilde{\rho}_h\right)\right] + Pe_1\left(\frac{1+\gamma}{1-\eta}\right) \frac{\partial}{\partial \tilde{z}}\left[\begin{array}{l} \dfrac{1+\gamma\tilde{\phi}}{\gamma} S_w c_w^l \tilde{v}_s - N_{sc}\dfrac{1+\gamma}{\gamma}\left(\dfrac{1+\gamma\tilde{\phi}}{1+\gamma\eta}\right)^8 \\ k_{rw}\left(\dfrac{\partial \tilde{p}_w}{\partial \tilde{z}} - 1\right) c_w^l + \dfrac{1+\gamma\tilde{\phi}}{\gamma} S_h c_w^h \tilde{\rho}_h \tilde{v}_s \end{array}\right] = 0 \quad \text{(A1)}$$

$$\text{I.C.: } \tilde{p}_w\left(\tilde{z},0\right) = \frac{\rho_w g D_0 + \rho_w g z}{\rho_w g L_t} = \frac{D_0}{L_t} + \tilde{z} \quad \text{(A2)}$$

$$\text{B.C. (1): } \tilde{p}_w\left(0,\tilde{t}\right) = \frac{D_0}{L_t} \quad \text{(A3)}$$

$$\text{B.C. (2): } \frac{\partial \tilde{p}_w}{\partial \tilde{z}}\left(D,\tilde{t}\right) = 1 \quad \text{(A4)}$$

where D_0 is seafloor depth and D is the bottom of the domain.

Methane Balance:

$$\frac{\partial}{\partial \tilde{t}}\left[\frac{1+\gamma\tilde{\phi}}{\gamma}\left(S_w\tilde{c}_m^l+S_h\tilde{c}_m^h\tilde{\rho}_h+S_g\tilde{c}_m^g\tilde{\rho}_g\right)\right]+Pe_1$$

$$\left(\frac{1+\gamma}{1-\eta}\right)\frac{\partial}{\partial \tilde{z}}\left[\begin{array}{l}\frac{1+\gamma\tilde{\phi}}{\gamma}S_w\tilde{c}_m^l\tilde{v}_s-N_{sc}\frac{1+\gamma}{\gamma}\left(\frac{1+\gamma\tilde{\phi}}{1+\gamma\eta}\right)^8\\ k_{rw}\left(\frac{\partial\tilde{p}_w}{\partial\tilde{z}}-1\right)\tilde{c}_m^l+\frac{1+\gamma\tilde{\phi}}{\gamma}S_h\tilde{c}_m^h\tilde{\rho}_h\tilde{v}_s\\ +\frac{1+\gamma\tilde{\phi}}{\gamma}S_g\tilde{c}_m^g\tilde{\rho}_g\tilde{v}_s-N_{sc}\frac{1+\gamma}{\gamma}\\ \left(\frac{1+\gamma\tilde{\phi}}{1+\gamma\eta}\right)^8k_{rg}\left(\frac{\partial\tilde{p}_g}{\partial\tilde{z}}-\tilde{\rho}_g\right)\frac{\mu_w}{\mu_g}\tilde{\rho}_g\tilde{c}_m^l\end{array}\right]$$

$$=\frac{\partial}{\partial\tilde{z}}\left[\frac{1+\gamma\tilde{\phi}}{\gamma}S_w\frac{\partial\tilde{c}_m^l}{\partial\tilde{z}}\right]+\frac{M_{CH_4}}{M_{org}}\tilde{\rho}_sDa\left(1-\tilde{\phi}\right)\tilde{\alpha}\beta \quad (A5)$$

I.C.: $\tilde{c}_m^l\left(\tilde{z},0\right)=0$ (A6)

B.C. (1): $\tilde{c}_m^l\left(0,\tilde{t}\right)=0$ (A7)

B.C. (2): $\frac{\partial\tilde{c}_m^l}{\partial\tilde{z}}\left(D,\tilde{t}\right)=1$ (A8)

Sediment Balance:

$$\frac{\partial}{\partial\tilde{t}}\left[1-\tilde{\phi}\right]+Pe_1\left(\frac{1+\gamma}{1-\eta}\right)\frac{\partial}{\partial\tilde{z}}\left[\left(1-\tilde{\phi}\right)\tilde{v}_s\right]=0$$

I.C.: $\tilde{v}_s\left(\tilde{z},0\right)=\frac{1-\eta}{1-\tilde{\phi}}$ (A9)

B.C. (1): $\tilde{v}_s\left(0,\tilde{t}\right)=1$ (A10)

Organic Balance:

$$\frac{\partial}{\partial\tilde{t}}\left[\left(1-\tilde{\phi}\right)\tilde{\alpha}\right]+Pe_1\left(\frac{1+\gamma}{1-\eta}\right)\frac{\partial}{\partial\tilde{z}}\left[\left(1-\tilde{\phi}\right)\tilde{v}_s\tilde{\alpha}\right]$$
$$=-Da\left(1-\tilde{\phi}\right)\tilde{\alpha}$$

I.C.: $\tilde{\alpha}\left(\tilde{z},0\right)=0$ (A11)

B.C. (1): $\tilde{\alpha}\left(0,\tilde{t}\right)=1$ (A12)

Initial porosity profile

Reduced porosity ($\tilde{\phi}$) is related to the dimensionless lithostatic stress ($\tilde{\sigma}_v$) and dimensionless pore pressure ($\tilde{p}_w$):

$$\tilde{\phi}=\eta\exp\left[-\frac{\tilde{\sigma}_v-\tilde{p}_w}{N_{t\phi}}\right] \quad (A13)$$

At hydrostatic pressure, the porosity profile can be computed as an analytical expression to serve as an initial condition:

$$\tilde{\phi}=\frac{\eta}{\eta+\left(1-\eta\right)\exp\left[\frac{\gamma\tilde{z}\left(\tilde{\rho}_s-1\right)}{N_{t\phi}\left(1+\gamma\right)}\right]} \quad (A14)$$